IEEE Access
Multidisciplinary | Rapid Review | Open Access Journal

Received 9 April 2024, accepted 12 May 2024, date of publication 20 May 2024, date of current version 30 May 2024.

Digital Object Identifier 10.1109/ACCESS.2024.3403106

RESEARCH ARTICLE

Adversarial-Learning-Based Taguchi Convolutional Fuzzy Neural Classifier for Images of Lung Cancer

CHENG-JIAN LIN[1], (Senior Member, IEEE), XUE-QIAN LIN[1], AND JYUN-YU JHANG[2]
[1]Department of Computer Science and Information Engineering, National Chin-Yi University of Technology, Taichung 41170, Taiwan
[2]Department of Computer Science and Information Engineering, National Taichung University of Science and Technology, Taichung 40401, Taiwan

Corresponding author: Cheng-Jian Lin (cjlin@ncut.edu.tw)

This work was supported in part by the National Science and Technology Council under Grant NSTC 112-2221-E-167-026.

ABSTRACT Deep learning technology has extensive application in the classification and recognition of medical images. However, several challenges persist in such application, such as the need for acquiring large-scale labeled data, configuring network parameters, and handling excessive network parameters. To address these challenges, in this study, we developed an adversarial-learning-based Taguchi convolutional fuzzy neural classifier (AL-TCFNC) for classifying malignant and benign lung tumors displayed in computed tomography images. In the framework of the developed AL-TCFNC, a fuzzy neural classifier replaces a conventional fully connected network, thereby reducing the number of network parameters and the training duration. To reduce experimental cost and training time, the Taguchi method was used. This method helps to identify the optimal combination of model parameters through a small number of experiments. The transfer learning of models across databases often results in subpar performance because of the paucity of labeled samples. To resolve this problem, we used a combination of maximum mean discrepancy and cross-entropy for adversarial learning with the proposed model. Two data sets, namely the SPIE–AAPM Lung CT Challenge data set and LIDC–IDRI Lung Imaging Research data set, were used to validate the AL-TCFNC model. When the AL-TCFNC model was used for transfer learning, it exhibited an accuracy rate of 89.55% and outperformed other deep learning models in terms of classification performance.

INDEX TERMS Lung cancer, computed tomography (CT), adversarial learning, convolutional neural network (CNN), fuzzy neural network, Taguchi method, maximum mean discrepancy.

I. INTRODUCTION

Computed tomography (CT) images are often used for the early detection of lung cancer, which commonly manifests as pulmonary nodules. These nodules may exhibit malignant or benign characteristics. Consequently, distinguishing between malignant and benign lung tumors is an indispensable step in the early diagnosis of lung cancer. However, enhancing diagnostic and detection accuracy is a challenging task. Deep learning technology has been adopted for the identification and classification of lung tumors. This technology can be used for automatically extracting pertinent tumor features from lung CT images and is more effective and accurate than are traditional deep learning methods [1], [2], [3].

Zhang et al. [1] combined multiple convolutional neural network (CNN) models to construct an ensemble learner for the classification of pulmonary nodules. Hu et al. [2] proposed STN model with unsupervised learning method to label malignant lung cancer. Shen et al. [3] introduced an interpretable deep hierarchical semantic CNN to predict the

The associate editor coordinating the review of this manuscript and approving it for publication was Xu Jing.

malignancy of pulmonary nodules observed in CT images. However, these methods have certain limitations. For example, CNN models, because of their substantial number of parameters, necessitate high computational costs and a long training duration.

In CNN models, fully connected networks (FCNs) are frequently used as classifiers. Each neuron in the FCN connects to all neurons in the preceding layer, with each connection bearing a corresponding weight. During model training, these weights are adjusted to learn the mapping from input to output data. However, the weights lack physical meaning. The fuzzy neural network (FNN) [4], [5] has wide-ranging applications across various domains. This neural network is endowed with fuzzy inference abilities; it seamlessly integrates the learning abilities of a neural network with the inferential capabilities of human thought, which are rooted in fuzzy logic [6]. Cheng et al. [7] introduced a novel fuzzy neural network that incorporates traditional convolution layers and fuzzy rule layers. The convolution layers extract discriminative features across scales, providing information for pixel-level features. The fuzzy rule layers adeptly handle various uncertainties, thereby ensuring robust segmentation outcomes.

The parameter settings of CNN models have a strong influence on their performance. Because extensive experimentation is essential for identifying a suitable parameter combination, this process demands substantial time and resource investments. The uniform distribution method [8] and Taguchi method [9] are commonly applied for setting parameters. These systematic methods facilitate the exploration and optimization of parameter settings to ensure optimal model performance. In the uniform distribution method, multiple variables are tested to identify the most favorable parameter combination for achieving the desired performance [8]. By contrast, in the Taguchi method, a relatively small number of experiments are performed, and a systematic experimental design is used to identify the primary factors influencing quality and their optimal setting. The aforementioned methods help to conserve time and resources while preserving model stability and performance [9].

Traditional machine learning methods operate under the assumption that data originate from the same distribution during the training and testing phases. However, real-world data might exhibit different distributions because of varying domains, environmental conditions, or time points. Thus, when different data sets are used, data relabeling becomes imperative, which necessitates considerable human effort and time. Domain adaptation, which is a key trend in the realms of machine learning and deep learning, is aimed at extracting features from source- and target-domain data with different distributions. These features are then mapped to a common feature space, thereby enabling the model to perform generalization effectively [10], [11]. Gallego et al. [12] proposed an incremental strategy for the adversarial learning of neural networks. This method involves self-labeling data from the target domain to the source domain making adversarial learning to extract new features. Liu et al. [13] proposed a multisource transfer learning method based on domain adversarial neural networks for the classification of electroencephalograms. Tzeng et al. [14] incorporated an adaptation layer into a CNN model. The output of the adaptive layer mitigated distribution disparities between the source and target domains and minimized classification losses in the source domain. However, under challenges such as category imbalance and extreme disparities between the source and target domains, model training might become unstable, thereby compromising the realization of optimal transfer effects. Gangeh et al. [15] developed a computer-aided tomography system for evaluating patients with locally advanced breast cancer who were receiving neoadjuvant chemotherapy. They used patient response monitoring data to explore kernel-based metrics for maximum mean discrepancy (MMD). This approach facilitates learning from imbalanced data and supervised learning based on random undersampling. Although the aforementioned method has high efficacy, it involves extensive parameter computations. In summary, domain adaptation—a key avenue of research within the domains of machine learning and deep learning—can help to address the complexities arising from disparate data distributions in real-world settings. By leveraging diverse adversarial learning techniques, domain adaptation can enhance model generalization across multiple domains.

In the present study, we developed an adversarial-learning-based Taguchi convolutional fuzzy neural classifier (AL-TCFNC) for the classification of malignant and benign lung tumors displayed in CT images. The contributions of our study are as follows:

1. In the developed AL-TCFNC, a fuzzy neural classifier (FNC) replaces an FCN, thereby reducing the number of network parameters and training duration.

2. Recognizing that fine-tuning the parameters of a deep learning model necessitates extensive experimentation, we used the Taguchi method to select the optimal parameter combination through a small number of experiments.

3. Given that the transfer learning of models across diverse databases results in poor performance because of the insufficiency of labeled samples, we combined MMD and cross-entropy (CE) in our adversarial learning strategy.

The rest of this paper is organized as follows. Section II presents an overview of the developed system architecture for the classification of lung tumors. Section III presents the experimental outcomes and comparisons between our method and alternative approaches. Finally, Section IV presents the conclusions of this study.

II. MATERIALS AND METHODS

Fig. 1 illustrates the developed system architecture for the classification of lung tumors. First, we used the Taguchi method to identify the optimal parameter combination for the proposed AL-TCFNC model. Next, we implemented the optimal parameter combination in this model to

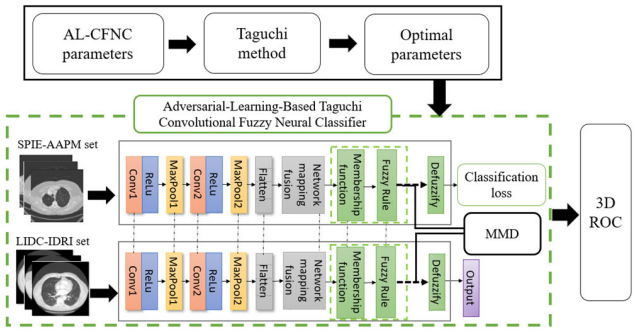

FIGURE 1. Overall system architecture developed for lung tumor classification.

classify malignant and benign lung tumors for evaluating the model's recognition performance. Finally, to apply the proposed model to transfer learning across different databases, we used the MMD method, thereby facilitating the transfer of knowledge acquired from the source domain to enhance classification performance in the target domain by minimizing the distribution disparity between the two domains. Specifically, the labeled SPIE–AAPM lung CT images are used as the source domain (Fig. 2(a)), and the unlabeled LIDC–IDRI lung CT images are adopted as the target domain (Fig. 2(b)). Our model's recognition performance was evaluated using a three-dimensional (3D) receiver operating characteristic (ROC) curve.

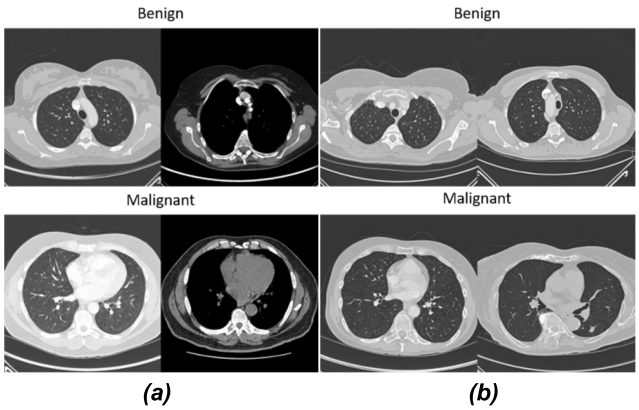

FIGURE 2. (a) SPIE-AAPM lung CT images. (b) LIDC-IDRI lung CT images.

A. ARCHITECTURE OF THE CONVOLUTIONAL FNC

The architecture of the convolutional FNC (CFNC) of the proposed model is depicted in Fig. 3. The CFNC comprises four distinct network layers: a convolutional layer, a pooling layer, a feature fusion layer, and an FNN layer. The convolutional layer extracts feature from lung CT images. The maximum pooling layer compresses these features to reduce the computational complexity and improve the calculation efficiency. The feature fusion layer combines individual features in a feature map, thereby integrating feature correlations to obtain representative features. The FNN layer

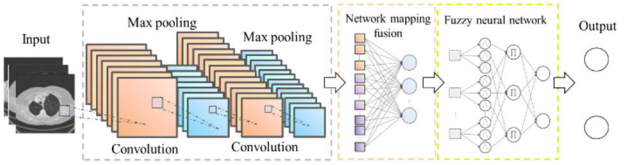

FIGURE 3. Convolutional FCN.

replaces the FCN layer and identifies semantic relationships between features and outputs. Notably, the use of the FNN layer effectively reduces the number of network parameters while enhancing the interpretability of feature–classification associations.

Convolutional operations often engender a sudden increase in network features. Researchers have used various feature fusion methods [16], [17] for reducing the volume of feature information. The network mapping fusion method [16] involves flattening the feature matrix and assigning a distinct weight to each feature element; these weights are subsequently fused (Fig. 4). The fusion formula for network mapping is as follows:

$$f_k = \sum_{j=1}^{m} \sum_{i=1}^{n} \left(W_{kij} * x_{ij} \right), \tag{1}$$

where f_k is the output of the kth fusion process, n is the number of input features of the mth channel layer, x_{ij} is the ith input feature element of the jth channel, and W_{kij} is the ith input weight of the jth channel in the kth fusion result.

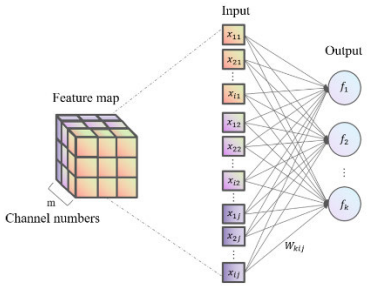

FIGURE 4. Schematic of the network mapping layer.

An FNN combines the learning ability of a neural network and the human-like inferencing ability of fuzzy logic. We used If–Then fuzzy rules to express. These rules map the fuzzified values of features to corresponding conclusion values.

Rule$_j$: IF f_1 is F_{1j} and f_2 is F_{2j} ...and f_k is F_{kj} ...and f_n is F_{nj}

$$THEN\ y\ is\ w_j, \tag{2}$$

where f_k is the input of the kth dimension, F_{kj} is the fuzzy set, w_j is the output weight, n is the number of input dimensions, and m is the number of fuzzy rules. A schematic of an FNN is displayed in Fig. 5.

The Gaussian membership function [17] is used to fuzzify each input for generating the corresponding

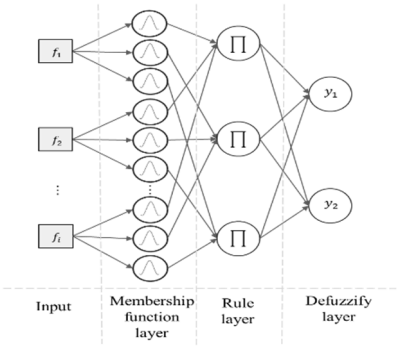

FIGURE 5. Schematic of an FNN.

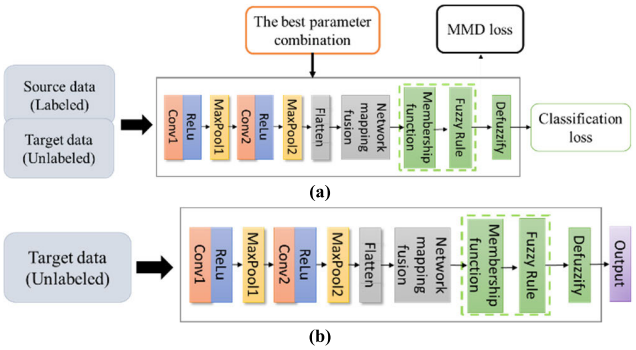

FIGURE 6. Architecture of the proposed AL-TCFNC model. (a) Use of the source and target domains for adversarial-learning-based training. (b) Use of only the target domain for validation.

membership degree. Membership values of 0 and 1 indicate feature importance, with 0 indicating nonsignificance and 1 indicating importance. The formula for calculating membership values is as follows:

$$\mu_{ij}(f) = exp\left(-\frac{[f_i - m_{ij}]^2}{\sigma_{ij}^2}\right), \tag{3}$$

where f_i is the input, and m_{ij} and σ_{ij} are the mean and deviation of Gaussian membership functions, respectively.

The attribution degrees corresponding to the inputs are combined, and the excited strength of each fuzzy rule is obtained as follows:

$$R_j = \prod_{i=1}^{n} \mu_{ij}, \tag{4}$$

Finally, the output of each rule is used as an input for the defuzzification layer to obtain a precise output. The relevant formula is as follows:

$$y_k = \sum_{j=1}^{m} R_j w_{jk}, \tag{5}$$

where y_k is kth output, R_j is the excited strength of jth fuzzy rule, and w_{jk} is the weight of the output.

B. ADVERSARIAL LEARNING METHODS

Real-world data often exhibit variations in distribution across different domains, environmental conditions, or time points. Adapting to such disparities typically demands labor-intensive data relabeling and learning efforts. In the case of medical images, clinicians must label the data. In this context, domain adaptation methods offer a solution by allowing the extraction of features from source- and target-domain data with different distributions and the mapping of the feature vectors of these data to a shared feature space, thereby enhancing the model's generalization performance.

In domain adaptation, the difference between the distributions of source- and target-domain data is crucial. MMD [18] is commonly used for measuring the difference between two feature distributions. The premise of this approach is that if the data distributions in the source and target domains are similar, these distributions have similar representations in the feature space. Fig. 6(a) illustrates the use of the source and target domains for adversarial-learning-based training in the proposed AL-TCFNC model, whereas Fig. 6(b) illustrates the use of only the target domain for validation.

The feature vectors generated from the source-domain data set (D_s) and target-domain data set (D_t) on the basis of the rule excitation degree of the FNN layer are expressed as follows, respectively (Fig. 6a): D_s=($s_1, s_2, \ldots, s_i$) and $D_t = (t_1, t_2, \ldots, t_j)$. The two data sets exhibit different distributions, and a kernel function is used to measure the difference in data distribution.

Given that the distributions of source- and target-domain data differ in Euclidean space, data are mapped to a high-dimensional space. To bring the two data distributions closer, the source- and target-domain data are mapped to the reproducing kernel Hilbert space [19]. In practice, the Gaussian kernel function is used for distance operations in the feature space, which eliminates the need for the direct computation of inner products in high-dimensional space. The Gaussian kernel function (K) is defined as follows:

$$K(a, b) = exp(\frac{-\|a-b\|^2}{2\sigma^2}), \tag{6}$$

where a and b are sample vectors in the source- or target-domain data sets, $\|a-b\|^2$ is the square of the Euclidean distance between the two vectors, and σ is the standard deviation of the Gaussian kernel, which regulates the kernel function width.

The Gaussian kernel function enables the measurement of the similarity between two data sets. When the distance between data points is small and the standard deviation is large, the Gaussian kernel function approaches 1, which indicates high similarity. However, as the distance increases or the standard deviation decreases, the Gaussian kernel function gradually decreases, which indicates reduced similarity between data points. Notably, the selection of the standard deviation for the Gaussian kernel function influences the results, with a smaller standard deviation resulting in the peaking of the kernel function. In essence, the peaking effect has a considerable influence classification performance when the local structure and data similarities are emphasized. Conversely, a larger standard deviation flattens the Gaussian

kernel function, which enhances overall data similarity and prevents a sole focus on local variations.

The features obtained after mapping the source and target domains are denoted as $\phi(x)$ and $\phi(y)$, respectively. Because $\phi(x)$ and $\phi(y)$ have infinite dimensions, the Gaussian kernel function is used to calculate the mean vectors in the feature space for the source- and target-domain data sets. The definition of MMD focuses primarily on the similarity between samples. MMD can be calculated as follows:

$$\begin{aligned} &MMD^2\left(D_s, D_t\right) \\ &= \left\| \frac{1}{m}\sum_{i=1}^{m}\phi\left(s_i\right) - \frac{1}{n}\sum_{j=1}^{n}\phi\left(t_j\right) \right\|_H^2 \\ &= \frac{1}{m^2}\sum_{i=1}^{m}\sum_{i'=1}^{m}K\left(s_i, s_i'\right) - \frac{2}{mn}\sum_{i=1}^{m}\sum_{j=1}^{n}K\left(s_i, t_j\right) \\ &\quad + \frac{1}{n^2}\sum_{j=1}^{n}\sum_{j'=1}^{n}K\left(t_j, t_j'\right), \end{aligned} \tag{7}$$

where D_s and D_t denoted source domain and target domain data, respectively; s and t are subset of D_s and D_t; $\emptyset(\cdot)$ is the mapping function that maps original values to Reproducing Kernel Hilbert Space (RKHS); the norm $\|\cdot\|_H$ is defined with respect to the specific Hilbert space associated with a reproducing kernel K; and H represents the space of functions in the Hilbert space.

During adversarial learning, MMD loss and CE are used to update the weights of the FNN. This approach minimizes the difference in feature distribution between the source and target domains and reduces the classification loss in the source domain. The overall loss function is expressed as follows:

$$L = Lc\left(D_s, y\right) + \lambda MMD^2\left(D_s, D_t\right), \tag{8}$$

In Eq. (8), the former term is the classification loss obtained after model training in the source domain and the latter term is the sum of MMD distances calculated after the rule layer. The hyperparameter λ is a penalty parameter.

During the parameter learning process, the distribution difference between the source and target domains is reduced by minimizing the MMD loss. Thus, the knowledge and features of the source domain can be mapped to those of the target domain by enhancing the model's recognition performance in the target domain. The trainable parameters in the AL-CFNC model are m_{ij}, σ_{ij}, and w_j, which are adjusted using a backpropagation learning algorithm. The following formula is used for parameter modification:

$$w_j\left(t+1\right) = w_j\left(t\right) - \eta\Delta w_j \tag{9}$$

$$m_{ij}(t+1) = m_{ij} - \eta_m \Delta m_{ij} \tag{10}$$

$$\sigma_{ij}(t+1) = \sigma_{ij} - \eta_\sigma \Delta\sigma_{ij} \tag{11}$$

where

$$\begin{aligned} \Delta w_j &= \frac{\partial L_c}{\partial w_j} = \frac{\partial L_c}{\partial y}\frac{\partial y}{\partial w_j} = \frac{\partial \frac{1}{2}(y-y_d)^2}{\partial y}\frac{\partial \sum_{j=1}^{m} R_j w_{jk}}{\partial w_j} \\ &= (y - y_k)R_j \end{aligned} \tag{12}$$

$$\begin{aligned} \Delta m_{ij} &= \frac{\partial L}{\partial m_{ij}} = \frac{\partial L}{\partial \mu_{ij}}\frac{\partial \mu_{ij}}{\partial m_{ij}} = \frac{\partial L}{\partial R_j}\frac{\partial R_j}{\partial \mu_{ij}}\frac{\partial \mu_{ij}}{\partial m_{ij}} \\ &= \frac{\partial L}{\partial \hat{y}}\frac{\partial \hat{y}}{\partial R_j}\frac{\partial R_j}{\partial \mu_{ij}}\frac{\partial \mu_{ij}}{\partial m_{ij}} = \left[(y - y_k) R_j w_j + \left\| \frac{1}{m}\sum_{i=1}^{m} \right. \right. \\ &\quad \left. \left. \times\phi\left(s_i\right) - \frac{1}{n}\sum_{j=1}^{n}\phi\left(t_j\right) \right\|_H^2 \right] \left[\frac{2\left[f_i - m_{ij}\right]^2}{\sigma_{ij}^2} \right] \end{aligned} \tag{13}$$

$$\begin{aligned} \Delta\sigma_{ij} &= \frac{\partial L}{\partial \sigma_{ij}} = \frac{\partial L}{\partial \mu_{ij}}\frac{\partial \mu_{ij}}{\partial \sigma_{ij}} = \frac{\partial L}{\partial R_j}\frac{\partial R_j}{\partial \mu_{ij}}\frac{\partial \mu_{ij}}{\partial \sigma_{ij}} \\ &= \frac{\partial L}{\partial \hat{y}}\frac{\partial \hat{y}}{\partial R_j}\frac{\partial R_j}{\partial \mu_{ij}}\frac{\partial \mu_{ij}}{\partial \sigma_{ij}} = \left[(y - y_k) R_j w_j + \left\| \frac{1}{m}\sum_{i=1}^{m} \right. \right. \\ &\quad \left. \left. \times\phi\left(s_i\right) - \frac{1}{n}\sum_{j=1}^{n}\phi\left(t_j\right) \right\|_H^2 \right] \left[\frac{2\left[f_i - m_{ij}\right]^2}{\sigma_{ij}^3} \right] \end{aligned} \tag{14}$$

where η_w, $\eta_{m,}$ and η_σ are the learning rates of w_j, m_{ij}, and σ_{ij}, respectively.

III. RESULTS

We used the AL-TCFNC model to assess the efficacy of the Taguchi method in optimizing parameter combinations and to evaluate the generalization ability of domain adaptation. Moreover, we compared the proposed model with other common deep learning models to evaluate its usefulness.

A. DATA SETS AND EVALUATION INDICATORS

In this study, two datasets were utilized: the SPIE-AAPM Lung CT Challenge dataset [20] and the open LIDC-IDRI Lung Imaging Research dataset [21]. The source domain input consisted of a total of 22,489 annotated SPIE-AAPM lung CT images, including 11,082 benign cases and 11,407 malignant cases, while the target domain input comprised 16,471 unannotated LIDC-IDRI lung CT images, consisting of 5,332 benign cases and 11,139 malignant cases. Maximum Mean Discrepancy (MMD) and Cross-Entropy (CE) were employed for adversarial learning. Finally, the unannotated LIDC-IDRI lung CT images were used for model validation.

The following indicators were used to assess the classification results: accuracy, true positive rate (TPR), false positive rate (FPR), and F1 score. We generated an ROC curve [22] and calculated the area under the ROC curve (AUC). Typically, in a binary classification model, the classifier assigns a score to each sample. A higher score indicates a higher likelihood of being positive. By varying the decision thresholds, we classified the samples into positive and negative categories, thereby obtaining different performance metrics (Fig. 7).

The two-dimensional (2D) ROC curve displayed in Fig. 8(a) characterizes the model performance at a single decision threshold and describes the relationship between FPR and TPR at various thresholds. In this study, FPR was determined as 1 − specificity. A higher specificity

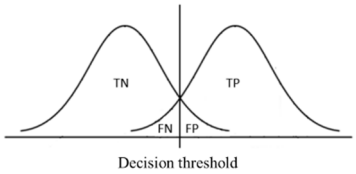

FIGURE 7. Decision threshold.

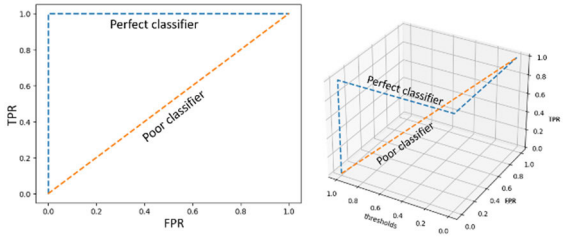

FIGURE 8. (a) 2D ROC and (b) 3D ROC curve.

corresponds to a lower FPR, which indicates an enhanced ability of the model to identify negative samples correctly. A higher AUC value implies that when the classifier randomly selects a positive sample, the classifier is more likely to correctly identify the sample as a positive sample than as a negative sample. Therefore, a higher AUC value correlates with a higher classifier accuracy.

Medical imaging frequently involves combined detection–estimation tasks. To evaluate the performance of classification models in these tasks, various objective measures have been proposed, such as accuracy, precision, and F1 score. An ROC curve is a visual tool for comparing classification models [23], [24], [25]. Guo et al. [24] conducted 3D ROC curve analysis and found that the combination of linearly constrained minimum variance with 3D ROC analysis can solve background problems caused by unknown complexity. Subsequently, by regarding small classes as signals to be detected, their class accuracy can be interpreted as a measure of signal detection capability or probability. Therefore, 3D ROC analysis can help to address class imbalance problems. Chang [25] analyzed the three 2D ROC curves and developed six quantitative classification measures on the basis of the AUC values of these curves. These quantitative classification measures can be used for comprehensively evaluating classifier performance. The concept of a 3D ROC curve usually refers to an extension of the traditional 2D ROC curve to include a third dimension, often representing the performance of a classifier at different decision thresholds. In 3D ROC space, metrics include sensitivity, specificity, and threshold. Similar to 2D ROC, we can evaluate the curvature of the ROC curve along the third dimension (e.g., decision threshold). A convex shape may indicate that a balanced model performs well across different trade-offs, while a concave shape may indicate a bias toward certain thresholds. Furthermore, the performance of the model changes as the decision threshold changes. Smooth and continuous transitions between different sensitivity and specificity values indicate that the model maintains discriminative power over a range of thresholds. The classification curve of perfect 3D ROC is shown in Fig. 8(b). The closer to the blue line, the better the classification performance.

B. OPTIMAL PARAMETER COMBINATION FOR THE AL-TCFNC MODEL

In the initial experiment, the size of the input image was set as $50 \times 50 \times 3$ pixels, and two sets of convolutional and pooling layers were used for feature extraction. Each convolutional layer used an initial convolution kernel (size: 3×3) for feature extraction and a max pooling layer (size: 2×2) for feature compression to reduce computational load. In the convolutional layer, 16 and 32 convolution kernels were used to extract various feature combinations. In the feature fusion layer, the network mapping method was used to reduce feature dimensions, which resulted in 32 features being obtained. These features were incorporated into the FNN for classifying malignant and benign lung tumors. For model training, the Adam optimizer was used; the learning rate, epoch count, and batch size were set as 0.001, 30, and 64, respectively.

In a Taguchi experiment, seven factors of the proposed model were explored to identify the optimal parameter combination. The following inference factors were selected for exploration: penalty parameter (λ), number of convolution filters in the first convolutional layer (C1_F), convolution kernel size of the first convolutional layer (C1_KS), number of convolution filters of the second convolutional layer (C2_F), convolution kernel size of the second convolutional layer (C2_KS), number of network mapping layers (NML), and number of fuzzy rules (FR). The levels of these factors were set as follows: λ—0.1, 0.2, 0.5, 0.6, 0.8, and 1.0; C1_F—16, 32, and 48; C1_KS—3, 5, and 7; C2_F—32, 48, and 64; C2_KS—3, 5, and 7; NML—32, 48, and 64; and FR—32, 48, and 64. Because of the combination of the seven factors and its levels, the traditional method necessitates $6^1 \times 3^6 = 4374$ experiments, whereas the Taguchi method necessitates only 18 experiments. To obtain stable results, each experiment with the same parameter combination was performed three times, denoted as y1, y2, and y3, respectively. The yave represents the average accuracy of three experimental results (i.e., y1, y2, and y3). The average accuracy was used to calculate the signal-to-noise (S/N) ratio and the loss function was larger-the-better. The formula of S/N is as follows:

$$\mathrm{S/N} = -10\log\left(1/n \sum_{i=1}^{n} \frac{1}{y_i}\right), \tag{15}$$

where n is the number of experiments and y_i is the accuracy of ith experiment with the same parameter combination. In this study, n is set as 3. The results of 18 experiments using the Taguchi method are summarized in Table 1.

The S/N ratio for each experiment was used to derive the average S/N ratio for each factor and level and to determine

TABLE 1. S/N ratios in the taguchi experiment.

Exp No.	Factors							Results				
	A	B	C	D	E	F	G					
	λ	C1_F	C1_KS	C2_F	C2_KS	NML	FR	$y1$	y2	y3	yave	S/N ratio
1	0.1	16	3	32	3	32	32	79.02%	81.99%	82.74%	81.25%	-1.808
2	0.1	32	5	48	5	48	48	82.89%	84.08%	84.52%	83.83%	-1.532
3	0.1	48	7	64	7	64	64	83.48%	85.12%	83.04%	83.88%	-1.528
4	0.2	16	3	48	5	64	64	81.70%	81.40%	83.04%	82.05%	-1.719
5	**0.2**	**32**	**5**	**64**	**7**	**32**	**32**	**85.86%**	**88.84%**	**88.69%**	**87.80%**	**-1.133**
6	0.2	48	7	32	3	48	48	81.85%	81.70%	82.00%	81.85%	-1.739
7	0.5	16	5	32	7	48	64	83.63%	83.78%	80.86%	82.76%	-1.647
8	0.5	32	7	48	3	64	32	82.44%	83.18%	82.59%	82.74%	-1.646
9	0.5	48	3	64	5	32	48	82.89%	82.44%	80.21%	81.85%	-1.742
10	0.6	16	7	64	5	48	32	83.48%	80.21%	81.70%	81.80%	-1.748
11	0.6	32	3	32	7	64	48	82.89%	80.06%	82.74%	81.90%	-1.738
12	0.6	48	5	48	3	32	64	82.89%	83.63%	85.86%	84.13%	-1.504
13	0.8	16	5	64	3	64	48	81.25%	83.18%	85.57%	83.33%	-1.589
14	0.8	32	7	32	5	32	64	85.12%	84.37%	84.23%	84.57%	-1.455
15	0.8	48	3	48	7	48	32	82.74%	84.08%	83.78%	83.53%	-1.563
16	1.0	16	7	48	7	32	48	83.18%	84.67%	83.04%	83.63%	-1.553
17	1.0	32	3	64	3	48	64	79.46%	78.87%	80.56%	79.63%	-1.979
18	1.0	48	5	48	5	64	32	82.59%	83.33%	82.74%	82.89%	-1.630

TABLE 2. Significance rank of each factor, optimal level of each parameter, and optimal parameter combination.

Level	A	B	C	D	E	F	G
1	-1.623	-1.678	-1.759	-1.670	-1.711	-1.533	-1.589
2	-1.531	-1.581	-1.506	-1.587	-1.638	-1.702	-1.649
3	-1.679	-1.618	-1.612	-1.620	-1.527	-1.642	-1.639
4	-1.664	—	—	—	—	—	—
5	-1.536	—	—	—	—	—	—
6	-1.721	—	—	—	—	—	—
Deviation	0.190	0.097	0.253	0.083	0.184	0.169	0.060
Ranking	2	5	1	6	3	4	7
The best level of each factor	2	2	2	2	3	1	1
The best parameter combination	0.2	32	5	48	7	32	32

the between-level numerical differences. Table 2 presents the significance rank of each factor, the optimal level of each parameter, and the best parameter combination. With the exception of λ, C1_F, C1_KS, C2_F, C2_KS, NML, and FR each have three levels. Hence, the presence of the "-" symbol in Table 2 indicates the unavailability of the corresponding value. Notably, λ, C1_KS, C2_KS, and NML exerted significant effects on the model. The maximum difference value of C1_KS, namely 0.252, indicates its key role in model response.

In Table 1, Experiment 5 shows a higher signal-to-noise ratio, which indicates that the parameters configured in Experiment 5 (i.e., $\lambda = 0.2$, C1_F = 32, C1_KS = 5, C2_F = 64, C2_KS = 7, NML = 32, FR = 32) is better than other experiments. But, this is not the best parameter combination for our method. We must analyze each factor and its level in 18 experiments through Table 2. Table 2 show that the factors affecting the S/N ratios based on yield extraction method are affected for each level of the parameters. The most significant factors can be determined by the larger difference in the S/N ratio. Finally, the best parameter combination in the ninth and tenth rows of Table 2 was set as $\lambda = 0.2$, C1_F = 32, C1_KS = 5, C2_F = 48, C2_KS = 7, NML = 32, and FR = 32. The obtained results were then compared

with those of the unoptimized AL-CFNC model. As demonstrated in Table 3, the accuracy, sensitivity, specificity, and F1 score of the AL-TCFNC model are 88.69%, 87.50%, 90.00%, and 89.02%, respectively. The proposed AL-TCFNC model outperforms the AL-CFNC model.

TABLE 3. Performance metrics of the AL-CFNC and AL-TCFNC model.

Models	Accuracy	Sensitivity	Specificity	F1-score
AL-CFNC	81.99%	81.53%	82.50%	82.59%
AL-TCFNC	88.69%	87.50%	90.00%	89.02%
Deviation	6.70%	5.97%	7.50%	6.42%

We performed 3D ROC analysis to evaluate the performance of the AL-TCFNC model. A 3D ROC curve comprises three 2D ROC curves: those of (P_D, τ), (P_F, τ), and (P_D, P_F). Therefore, we plotted 3D ROC curves for the AL-CFNC and AL-TCFNC models by using three parameters, namely P_D, P_F, and τ where denoted TPR, FPR, and thresholds, respectively; the step size of τ was 0.01 in our experiments. Fig. 9(b) presents the 3D ROC curves for the AL-CFNC and AL-TCFNC models. The results indicate that the optimal parameter combination markedly enhanced classifier accuracy. Fig. 9(a) indicates that the AL-TCFNC and AL-CFNC models had the same AUC values in the 2D ROC curves, and identifying the superior model on the basis of these curves was difficult. However, the 2D ROC curves clearly indicated that the AL-TCFNC model had higher performance than did the AL-CFNC model, as the curve of AL-TCFNC is closer to the perfect curve, as Fig 8(a). The 3D ROC curves indicated that the AL-TCFNC model had better stability which means that under different thresholds excellent P_D and P_F. In other words, the proposed AL-TCFNC model does not cause degradation in classification performance due to changes in different thresholds. Illustrated in Fig 8(b), the 3D ROC curve (depicted by the blue line) for AL-TCFNC reveals that test accuracy improves as the curve approaches the upper left corner of the chart. This is attributed to the fact that in the upper left corner, sensitivity equals 1, and the false positive rate is 0 (with specificity equating to 1), signifying superior performance.

C. ADVERSARIAL LEARNING OF THE AL-TCFNC MODEL ACROSS DATABASES

For adversarial learning, we used the labeled SPIE–AAPM lung CT images as the source-domain input and combined the MMD and CE methods for adversarial learning. Subsequently, unlabeled LIDC–IDRI lung CT images were used for model validation. The optimal parameter combination, which was identified using the Taguchi method, was applied to the AL-TCFNC model. During the training process, we set the learning rate as 0.001, deviation as 2, and batch size as 64 and used the early stopping mechanism. Under the aforementioned conditions, the classification performance of the AL-TCFNC model was compared with that of several other common models, namely, LeNet-5 [26], VGG-16 [27], and AL-AlexNet (proposed by Tzeng et al.) [14]. The LeNet-5 [26] and VGG-16 [27] models that are incorporated into adversarial learning are referred to as AL-LeNet-5 and AL-VGG-16, respectively. The experimental results revealed that the AL-TCFNC model outperformed the AL-AlexNet, AL-LeNet-5, and AL-VGG-16 models in terms of accuracy, sensitivity, and F1 score. Furthermore, the number of parameters was considerably less for the AL-TCFNC model (0.266 MB) than for the AL-AlexNet (27.701 MB) and AL-VGG-16 (12.604 MB) models (Table 4).

TABLE 4. Adversarial learning data for various models.

Models	Accuracy	Sensitivity	Specificity	F1-score	Number of parameters (MB)
AL-AlexNet [14]	84.33%	77.14%	92.19%	83.72%	27.701
AL-LeNet-5 [26]	85.07%	75.71%	95.31%	84.12%	0.245
AL-VGG-16 [27]	85.82%	77.14%	95.31%	85.04%	12.604
AL-TCFNC	88.69%	87.50%	90.00%	89.02%	0.266

The 2D ROC and 3D ROC curves for various models are displayed in Fig. 10(a) and 10(b), respectively. As shown in Fig. 10(b) (3D ROC curve), the AL-TCFNC model achieved relatively high TPR and FPR values across different decision thresholds. In essence, the AL-TCFNC model exhibited a higher TPR and a lower FTR.

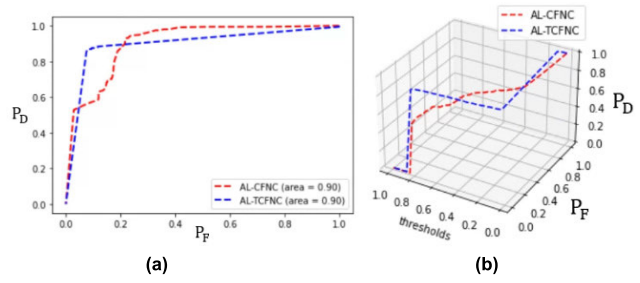

FIGURE 9. (a) 3D ROC and (b) 2D ROC curves for the AL-CFNC and AL-TCFNC models.

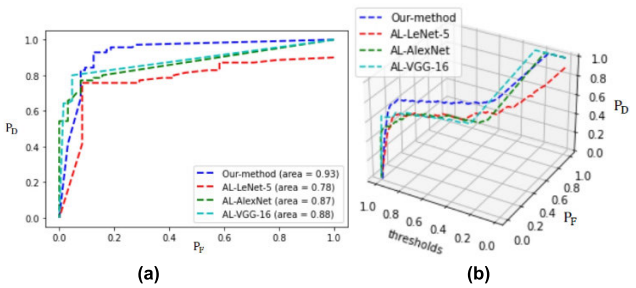

FIGURE 10. (a) 2D ROC and (b) 3D ROC curves for various models.

In our experiments, MMD played a pivotal role. By minimizing the distribution difference between source- and target-domain data, the knowledge acquired from the source domain was leveraged to enhance the model's performance in the target domain. Given that the selection of the standard deviation for the Gaussian kernel function influences the experimental outcomes, we performed multiple experiments by varying the standard deviation. Table 5 presents the experimental results for various models under standard deviations ranging from 2.0 to 7.0. These results indicate that the accuracy of the AL-TCFNC model surpassed that of other models. Notably, when the standard deviation was set as 5.0, the AL-TCFNC model achieved its highest accuracy (89.55%), which was 0.86% higher than its accuracy at the default standard deviation of 2.0.

TABLE 5. Accuracy of various models under different standard deviations.

Accuracy / Models	Deviation 2.0	3.0	4.0	5.0	6.0	7.0
AL-AlexNet [14]	81.34%	83.57%	83.58%	82.84%	82.09%	82.83%
AL-LeNet-5 [26]	83.17%	83.66%	83.17%	85.02%	84.65%	83.63%
AL-VGG-16 [27]	81.33%	83.58%	82.84%	85.07%	82.84%	83.54%
AL-TCFNC	88.69%	84.33%	85.07%	89.55%	88.06%	85.82%

Fig 11 shows the confusion matrix of AL-TCFNC. As can be seen from Fig 11, the correct classification accuracy of AL-TCFNC for benign lung cancer is 87.50%, and the correct classification accuracy for malignant lung cancer is 88.57%. These results highlight the effectiveness of AL-TCFNC using adversarial learning to accurately classify CT images within the target domain.

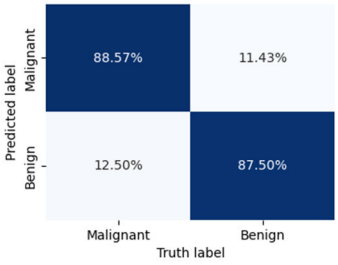

FIGURE 11. The confusion matrix of AL-TCFNC in lung carcer detection.

Table 6 illustrates the comparison results of the proposed AL-TCFNC and existing methods (i.e., Sharma et al. [29], Wu et al. [30], and Feng et al. [31]). In Table 6, the experiment employed two adversarial learning methods: supervised adversarial learning and unsupervised adversarial learning. In addition, two databases (i.e., SPIE–AAPM and LIDC–IDRI) were used for testing various methods. The evaluation metrics included accuracy, sensitivity, specificity, and F1-score. To evaluate the stability of AL-TCFNC,

TABLE 6. Adversarial learning data for various methods.

Models	Accuracy	Sensitivity	Specificity	F1-score
Supervised adversarial learning with k-fold cross-validation in SPIE–AAPM dataset				
Sharma et al. [29]	93.96%	94.46%	94.18%	94.40%
AL-TCFNC	99.66%	99.52%	99.79%	99.65%
Supervised adversarial learning with k-fold cross-validation in LIDC–IDRI dataset				
Wu et al. [30]	92.36%	91.62%	93.08%	92.25%
AL-TCFNC	97.94%	93.69%	99.93%	96.70%
Unsupervised adversarial learning				
Feng et al. [31]	75.72%	49.99%	84.90%	62.92%
AL-TCFNC	88.69%	87.50%	90.00%	89.02%

this experiment also introduced K-fold cross-validation and assessed its performance on lung CT images from SPIE-AAPM and LIDC-IDRI datasets. In this study, we set K to 5. Experimental results indicate the proposed AL-TCFNC in supervised adversarial learning achieved average accuracies of 99.66% and 97.94% in SPIE-AAPM and LIDC-IDRI datasets, respectively. However, the average accuracies of Sharma et al. [29] and Wu et al. [30] methods in the two data sets are 93.96% and 92.36%, respectively. In unsupervised adversarial learning, Feng et al. [31] achieved an accuracy of 75.72% using domain adversarial neural network approach. However, AL-TCFNC achieves an accuracy of 88.69% in unsupervised adversarial learning, which is 12.97 percentage points higher than that of the method of Feng et al. [31].

The above experiments demonstrate the effectiveness of the proposed method. However, there are still some challenges in real-world applications, such as generalization across datasets, model interpretability, statistical evaluation and validation, and clinical system implementation. Many studies have suggested addressing the issues of generalization across datasets and model interpretability by employing attention mechanisms [28] and the Gradient-weighted Class Activation Mapping (Grad-CAM) [32]. The attention mechanism can enhance the feature extraction and representation capabilities of the model, thereby further improving its overall performance. Grad-CAM can display the attention regions of the attention mechanism to explain the model's reasoning. Additionally, the accuracy, sensitivity, and specificity metrics used in assessment and analysis may be affected by the degree of learning, making performance metrics subjective. In this case, the fuzzy evaluation method [33] can be used to exclude outliers and make the evaluation data more valuable. Finally, for effective clinical application, chip-based systems are imperative. The chip-based system not only greatly improves the inference speed of the model, but also reduces the computing power consumption.

IV. CONCLUSION

In this study, we developed an AL-TCFNC model for the classification of malignant and benign lung tumors displayed in CT images. In this model, we substituted an FCN with an FNC to reduce the number of network parameters and the training duration. The Taguchi method was used to identify the optimal parameter combination through a small number of experiments. A combination of MMD and CE was leveraged for the adversarial learning of the proposed model. The use of the Taguchi experiment resulted in an accuracy value of 88.69%, which indicated a substantial improvement (by 6.70%) compared with the results obtained without the Taguchi experiment. Furthermore, a careful selection of an appropriate standard deviation ensured that the AL-TCFNC model attained an accuracy rate of 89.55% in transfer learning and surpassed the classification performance of other deep learning models. Notably, in 3D ROC analysis, the AL-TCFNC model consistently exhibited a higher TPR and lower FPR across different decision thresholds than other deep learning models in terms of classification performance, which reaffirmed that it had superior recognition accuracy and a reduced number of false positive instances.

Although the accuracy, sensitivity, specificity, and F1-score performance of the proposed AL-TCFNC method using different data sets in both supervised and unsupervised adversarial learning are better than other methods. This study has its limitations. In the Taguchi experiments, the influencing factors and their levels of the proposed AL-TCFNC were difficult to determine. The optimal parameter combination of the model may produce different results when different factors and their levels are selected. Therefore, more time is needed to determine these important factors and their levels. Furthermore, the evaluation metrics used in the experiments may bias the evaluation results due to outliers. In future research, we will consider introducing statistical evaluation and validation to make the experimental results more reliable.

REFERENCES

[1] B. Zhang, S. Qi, P. Monkam, C. Li, F. Yang, Y.-D. Yao, and W. Qian, "Ensemble learners of multiple deep CNNs for pulmonary nodules classification using CT images," *IEEE Access*, vol. 7, pp. 110358–110371, 2019.

[2] X. Hu, J. Yang, and J. Yang, "A CNN-based approach for lung 3D-CT registration," *IEEE Access*, vol. 8, pp. 192835–192843, 2020, doi: 10.1109/ACCESS.2020.3032612.

[3] S. Shen, S. X. Han, D. R. Aberle, A. A. Bui, and W. Hsu, "An interpretable deep hierarchical semantic convolutional neural network for lung nodule malignancy classification," *Expert Syst. Appl.*, vol. 128, pp. 84–95, Aug. 2019.

[4] M. Pratama, W. Pedrycz, and G. I. Webb, "An incremental construction of deep neuro fuzzy system for continual learning of nonstationary data streams," *IEEE Trans. Fuzzy Syst.*, vol. 28, no. 7, pp. 1315–1328, Jul. 2020.

[5] D. C. Li, M. Y. Lin, and L.-D. Chou, "Macroscopic big data analysis and prediction of driving behavior with an adaptive fuzzy recurrent neural network on the Internet of Vehicles," *IEEE Access*, vol. 10, pp. 47881–47895, 2022.

[6] O. Uncu and I. B. Turksen, "Discrete interval type 2 fuzzy system models using uncertainty in learning parameters," *IEEE Trans. Fuzzy Syst.*, vol. 15, no. 1, pp. 90–106, Feb. 2007.

[7] C. Guan, S. Wang, and A. W. Liew, "Lip image segmentation based on a fuzzy convolutional neural network," *IEEE Trans. Fuzzy Syst.*, vol. 28, no. 7, pp. 1242–1251, Jul. 2020.

[8] W.-H. Ho, T.-H. Huang, P.-Y. Yang, J.-H. Chou, J.-Y. Qu, P.-C. Chang, F.-I. Chou, and J.-T. Tsai, "Robust optimization of convolutional neural networks with a uniform experiment design method: A case of phonocardiogram testing in patients with heart diseases," *BMC Bioinf.*, vol. 22, no. S5, pp. 1–11, Nov. 2021.

[9] S.-F. Li, M.-L. Huang, and Y.-S. Wu, "Combining the Taguchi method and convolutional neural networks for arrhythmia classification by using ECG images with single heartbeats," *Mathematics*, vol. 11, no. 13, p. 2841, Jun. 2023.

[10] M. Wang and W. Deng, "Deep visual domain adaptation: A survey," *Neurocomputing*, vol. 312, pp. 135–153, Oct. 2018.

[11] Z. Chen, C. Chen, X. Jin, Y. Liu, and Z. Cheng, "Deep joint two-stream Wasserstein auto-encoder and selective attention alignment for unsupervised domain adaptation," *Neural Comput. Appl.*, vol. 32, no. 11, pp. 7489–7502, Jun. 2020.

[12] A.-J. Gallego, J. Calvo-Zaragoza, and R. B. Fisher, "Incremental unsupervised domain-adversarial training of neural networks," *IEEE Trans. Neural Netw. Learn. Syst.*, vol. 32, no. 11, pp. 4864–4878, Nov. 2021.

[13] D. Liu, J. Zhang, H. Wu, S. Liu, and J. Long, "Multi-source transfer learning for EEG classification based on domain adversarial neural network," *IEEE Trans. Neural Syst. Rehabil. Eng.*, vol. 31, pp. 218–228, 2023.

[14] E. Tzeng, J. Hoffman, N. Zhang, K. Saenko, and T. Darrell, "Deep domain confusion: Maximizing for domain invariance," 2014, *arXiv:1412.3474*.

[15] M. J. Gangeh, H. Tadayyon, L. Sannachi, A. Sadeghi-Naini, W. T. Tran, and G. J. Czarnota, "Computer aided theragnosis using quantitative ultrasound spectroscopy and maximum mean discrepancy in locally advanced breast cancer," *IEEE Trans. Med. Imag.*, vol. 35, no. 3, pp. 778–790, Mar. 2016.

[16] C.-J. Lin and J.-Y. Jhang, "Intelligent traffic-monitoring system based on YOLO and convolutional fuzzy neural networks," *IEEE Access*, vol. 10, pp. 14120–14133, 2022, doi: 10.1109/ACCESS.2022.3147866.

[17] C.-J. Lin and T.-Y. Yang, "A fusion-based convolutional fuzzy neural network for lung cancer classification," *Int. J. Fuzzy Syst.*, vol. 25, no. 2, pp. 451–467, Mar. 2023.

[18] A. Gretton, K. M. Borgwardt, M. Rasch, B. Schoklopf, and A. J. Smola, "A kernel method for the two-sample-problem," in *Proc. Adv. Neural Inf. Process. Syst.*, 2006, pp. 513–520.

[19] S. J. Pan, I. W. Tsang, J. T. Kwok, and Q. Yang, "Domain adaptation via transfer component analysis," *IEEE Trans. Neural Netw.*, vol. 22, no. 2, pp. 199–210, Feb. 2011.

[20] S. G. Armato et al., "SPIE-AAPM-NCI lung nodule classification challenge dataset," *Cancer Imag. Arch.*, 2017, doi: 10.7937/K9/TCIA.2015.UZLSU3FL.

[21] S. G. Armato et al., "The lung image database consortium (LIDC) and image database resource initiative (IDRI): A completed reference database of lung nodules on CT scans," *Med. Phys.*, vol. 38, no. 2, pp. 915–931, Jan. 2011.

[22] T. Saito and M. Rehmsmeier, "The precision-recall plot is more informative than the ROC plot when evaluating binary classifiers on imbalanced datasets," *PLoS ONE*, vol. 10, no. 3, Mar. 2015, Art. no. e0118432.

[23] A. Wunderlich, B. Goossens, and C. K. Abbey, "Optimal joint detection and estimation that maximizes ROC-type curves," *IEEE Trans. Med. Imag.*, vol. 35, no. 9, pp. 2164–2173, Sep. 2016.

[24] R. Guo, X. Shen, and X. Zhang, "3D ROC histogram: A new ROC analysis tool incorporating information on instances," *IEEE Access*, vol. 7, pp. 183396–183404, 2019.

[25] C.-I. Chang, "An effective evaluation tool for hyperspectral target detection: 3D receiver operating characteristic curve analysis," *IEEE Trans. Geosci. Remote Sens.*, vol. 59, no. 6, pp. 5131–5153, Jun. 2021.

[26] Y. Lecun, L. Bottou, Y. Bengio, and P. Haffner, "Gradient-based learning applied to document recognition," *Proc. IEEE*, vol. 86, no. 11, pp. 2278–2324, Nov. 1998.

[27] K. Simonyan and A. Zisserman, "Very deep convolutional networks for large-scale image recognition," in *Proc. 3rd Intl. Conf. Learning Represent. (ICLR)*, 2015, pp. 1–14.

[28] Z. Niu, G. Zhong, and H. Yu, "A review on the attention mechanism of deep learning," *Neurocomputing*, vol. 452, pp. 48–62, Sep. 2021.

[29] S. Sharma, P. Fulzele, and I. Sreedevi, "Hybrid model for lung nodule segmentation based on support vector machine and k-nearest neighbor," in *Proc. 4th Int. Conf. Comput. Methodologies Commun. (ICCMC)*, Mar. 2020, pp. 170–175.

[30] R. Wu, C. Liang, Y. Li, X. Shi, J. Zhang, and H. Huang, "Self-supervised transfer learning framework driven by visual attention for benign–malignant lung nodule classification on chest CT," *Expert Syst. Appl.*, vol. 215, Apr. 2023, Art. no. 119339.
[31] Y. Feng, Y. Luo, and J. Yang, "Cross-platform privacy-preserving CT image COVID-19 diagnosis based on source-free domain adaptation," *Knowl.-Based Syst.*, vol. 264, Mar. 2023, Art. no. 110324.
[32] R. R. Selvaraju, M. Cogswell, A. Das, R. Vedantam, D. Parikh, and D. Batra, "Grad-CAM: Visual explanations from deep networks via gradient-based localization," in *Proc. IEEE Int. Conf. Comput. Vis. (ICCV)*, Venice, Italy, Oct. 2017, pp. 618–626.
[33] T.-C. Chang, "A fuzzy evaluation approach to determine superiority of deep learning network system in terms of recognition capability: Case study of lung cancer imaging," *Ann. Oper. Res.*, pp. 1–21, 2023, doi: 10.1007/s10479-023-05299-1.

CHENG-JIAN LIN (Senior Member, IEEE) received the B.S. degree in electrical engineering from the Tatung Institute of Technology, Taipei, Taiwan, in 1986, and the M.S. and Ph.D. degrees in electrical and control engineering from National Chiao Tung University, Taiwan, in 1991 and 1996, respectively. Currently, he is a Chair Professor with the Computer Science and Information Engineering Department, National Chin-Yi University of Technology, Taichung, Taiwan. His current research interests include machine learning, pattern recognition, intelligent control, image processing, intelligent manufacturing, and evolutionary robots.

XUE-QIAN LIN received the B.S. degree from the Department of Computer Science and Information Engineering, National Chin-Yi University of Technology, Taichung, Taiwan, in 2021, where he is currently pursuing the master's degree. His current research interests include fuzzy neural networks, image processing, and machine learning.

JYUN-YU JHANG received the B.S. and M.S. degrees from the Department of Computer Science and Information Engineering, National Chin-Yi University of Technology, Taichung, Taiwan, in 2015, and the Ph.D. degree in electrical and control engineering from National Chiao Tung University, Taiwan, in 2021. He is currently an Assistant Professor with the Computer Science and Information Engineering Department, National Taichung University of Science and Technology, Taichung. His current research interests include fuzzy logic theory, type-2 neural fuzzy systems, evolutionary computation, machine learning, computer vision, and application.